Supporting Information

Stable magnetic skyrmion states at room temperature confined to corrals of artificial surface pits fabricated by a focused electron beam

Takao Matsumoto,[†] Yeong-Gi So,[‡] Yuji Kohno,[§] Yuichi Ikuhara,[†¶] and Naoya Shibata[†¶]*

[†]Institute of Engineering Innovation, School of Engineering, The University of Tokyo, 2-11-16 Yayoi, Bunkyo-ku, Tokyo 113-8656, Japan

[‡]Department of Materials Science, Graduate School of Engineering and Resource Science, Akita University, 1-1 Tegata Gakuen-machi, Akita, Akita 010-8502, Japan

[§]JEOL Ltd., 1-2, Musashino 3-chome Akishima, Tokyo 196-8558, Japan

[¶]Nanostructures Research Laboratory, Japan Fine Ceramic Center, 2-4-1 Mutsuno, Atsuta-ku, Nagoya 456-8587, Japan.

Corresponding Author *E-mail: (T.M.) takao.matsumoto@sogo.t.u-tokyo.ac.jp

MATERIALS AND METHODS

Bulk polycrystal preparation. A bulk polycrystalline β-Mn type $Co_8Zn_8Mn_4$ was synthesized from highly pure Co (99.99 %), Zn(99.99 %) and Mn(99.99 %) using an electric furnace; constituent elements with the nominal composition of $Co_8Zn_8Mn_4$ were sealed in an evacuated silica tube, heated at 1273 K for 12 h, subsequently cooled to 1198 K at a cooling rate of 1 K/h, and annealed at 1198 K for 72 h, followed by water-quenching.

Thin plate specimen preparation. The (111) thin plate was fabricated from a bulk crystal by using an Ion Slicer (IS9001, JEOL, Ltd.). Prior to observation, the thin plate was further polished with a plasma cleaner (Solarus, Model 950, Gatan, Inc.).

TEM/STEM observation. The thin plate specimen was first characterized by using a conventional TEM (JEM-2010HC, JEOL, Ltd.). To obtain atomic-resolution STEM images, we used an aberration-corrected STEM (JEM-200F, JEOL, Ltd.) equipped with a cold field emission gun operated at 200 kV. For DPC STEM observations, we used a STEM (JEM-2100F, JEOL, Ltd.) equipped with a probe-forming aberration corrector (CEOS, GmbH) and a Schottky field emission gun operated at 200 kV. This microscope was equipped with a segmented annular all field (SAAF) detector which is described in the previous literature in detail[3]. When observing magnetic skyrmion, the objective lens was switched off, and the illumination system was adjusted to obtain either probe size of 3.5 nm with a probe-forming aperture semi-angle of 0.426 mrad., respectively. Perpendicular magnetic field was applied by slightly exciting the objective lens, and the field strength was calibrated by using magnetic field measuring specimen holder equipped with three Hall-probe sensors. For a probe size of 3.5 nm, the detector ranges are 0.108-0.162 mrad and 0.244-0.422 mrad for DPC images and ADF images, respectively.

Surface pits fabrication. When fabricating isolated surface pits as shown in Figures 1-3, the objective lens was switched off, and the illumination system was adjusted as the same electron conditions as DPC STEM observations except a larger condenser aperture was used. When fabricating the linear surface pits as shown in Figures 4-6, the objective lens was strongly excited to form smaller probe size with increasing probe current. A custom program to control the scanning of the focused electron beam was written by Y.K.

Cross-sectional specimen preparation. A dummy in-plane (111) thin plate specimen was fabricated from a bulk crystal by using a FIB (NX2000, Hitachi High-Tech.). The thin plate specimen was finally polished by using 5 kV Ga ion beam with a current of 20 pA for 6 minutes, and then by using 1 kV Ar ion beam with a current of 20 nA for 3 minutes. Prior to observation, the thin plate was further polished with a plasma cleaner (Solarus, Model 950, Gatan, Inc.). Several linear surface pits were fabricated on the thin plate specimen. Next, a cross-sectional thin plate specimen containing the fabricated area was prepared by using a FIB (NX2000, Hitachi High-Tech.) equipped with micro-sampling apparatus.

Monte Carlo simulations. A single spin-flip Monte Carlo (MC) simulated annealing method was used to simulate the ground state. Periodic boundary conditions was used. Simulations begin from random distributions of magnetic moments at a sufficiently high temperature and then annealed to lower temperatures with a step of 10^4 MC steps. The grid size was 24. Interaction constants J and D are set as 1 meV and 0.797 meV, respectively. Only nearest neighbor interactions were considered and no anisotropy energy was included in the present study.

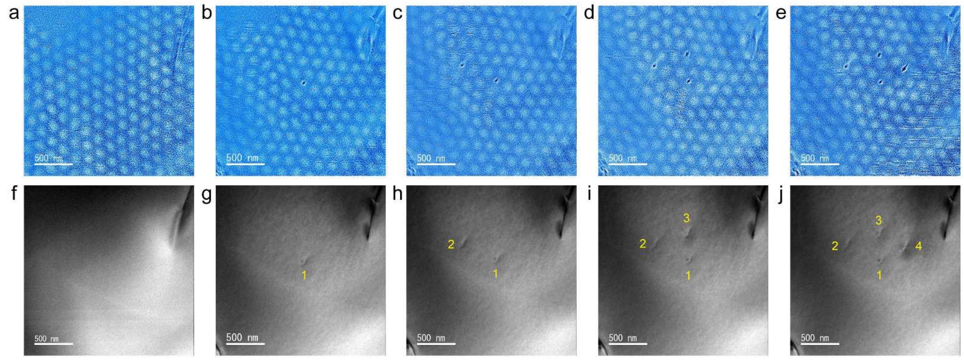

Figure S1. Sequential magnetic helicity images and ADF images showing interactions of skyrmions with four isolated surface pits created by a focused electron beam. (a)-(e) Magnetic helicity image and (f)-(j) corresponding ADF images with perpendicular magnetic field of 59.9 mT at a room temperature (295 K) are shown. Surface pits are sequentially numbered in (g)-(j). (a)(f) Prior to fabrication, a regular hexagonal skyrmion lattice was observed. (b)(g) When the first surface pit was created in the lattice, it created a lattice disorder. For all of the other three surface pits created, similar lattice disorders were created as individual skyrmions were affected by surface pits. The final state is shown in Figure 1. It should be noted here that it is essential to evaluate the influence by visualizing skyrmion and defects immediately after fabrication because we are observing skyrmion at a room temperature (T=295 K) close to the Curie temperature (Tc~300 K) of $Co_8Zn_8Mn_4$ where there are strong thermal fluctuations (T/Tc~0.98). Actually, the lattice orientation was observed to change frequently in the experiment.

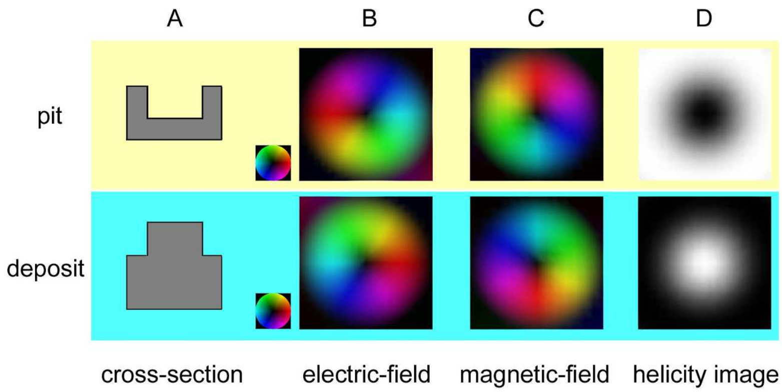

Figure S2. A schematic explanation on how a circular surface pit and a circular deposit on a thin plate specimen are imaged in DPC STEM. Note that only column A is cross-sectional while columns B-D are in-plane view. Thickness profiles of a circular surface pit and deposit as shown in column A produce electric field as shown in column B. The origin of the electric field is the change in the projected mean inner potential. Corresponding deflections of focused electron beam by each electric field are reconstructed as (virtual) magnetic field as shown in column C. Corresponding helicity images are shown in column D. In summary, a circular surface pit appears as a small skyrmion with clockwise (CW) in-plane spin rotation, while a circular deposit as a small skyrmion with counter-clockwise (CCW) in-plane spin rotation. Corresponding helicity images are a dark disk and a bright disk, respectively.

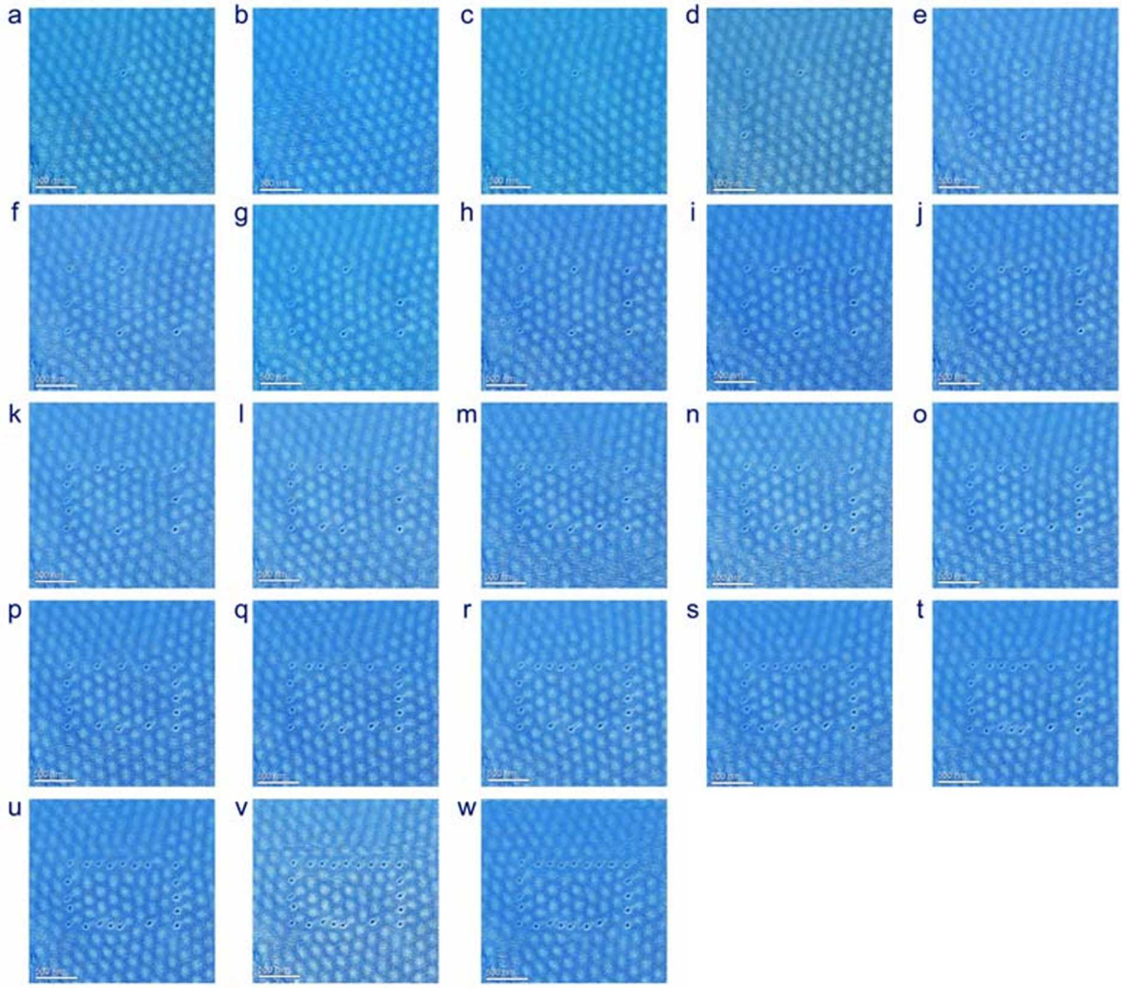

Figure S3. Sequential magnetic helicity images showing the continuous observation of the magnetic skyrmion state affected by a series of surface pits created by a focused electron beam as shown in Figure 2. Helicity images with perpendicular magnetic field of 59.9 mT at a room temperature (295 K) are shown. Every surface pit created lattice disorder in the skyrmion lattice just as shown in Figure 2 and Figure S1.

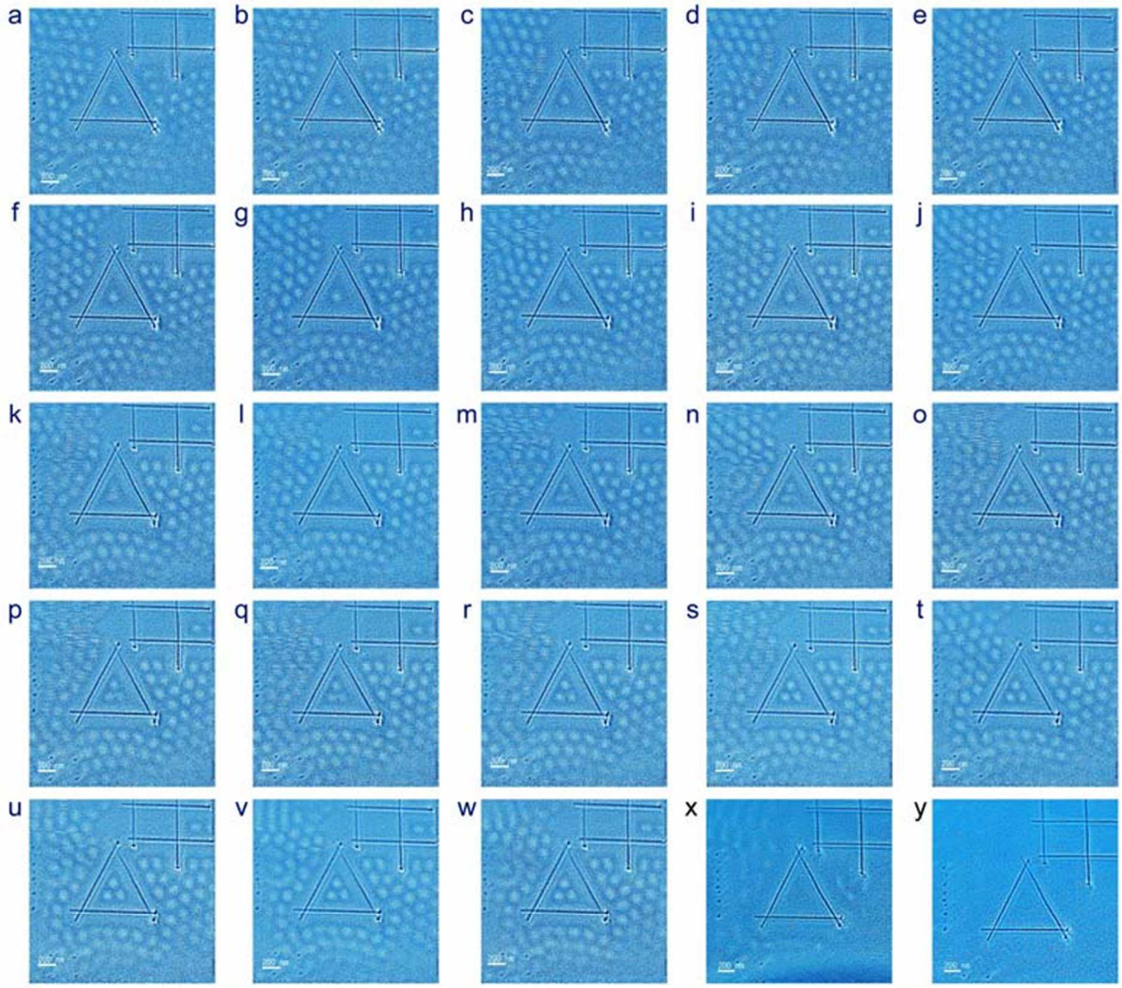

Figure S4. Sequential magnetic helicity images showing the transition of the magnetic skyrmion state in a triangular corral of surface pits as perpendicular magnetic field is changed. Helicity images at room temperature (295 K) with perpendicular magnetic field of (a) 59.9 mT, (b) 58.2 mT, (c) 56.2 mT, (d) 54.1 mT, (e) 52.1 mT, (f) 50.0 mT, (g) 48.0 mT, (h) 46.0 mT, (i) 43.8 mT, (j) 41.8 mT (k)-(o) 40.8 mT, (p) 39.8 mT, (q) 38.8 mT, (r) 37.8 mT, (s) 35.7 mT, (t) 33.7 mT, (u) 31.6 mT, (v) 29.5 mT, and (w) 27.5 mT are shown. As references, helicity images at room temperature (295 K) with perpendicular magnetic field of (x) 76.6 mT, and (y) 109.2 mT are also shown.

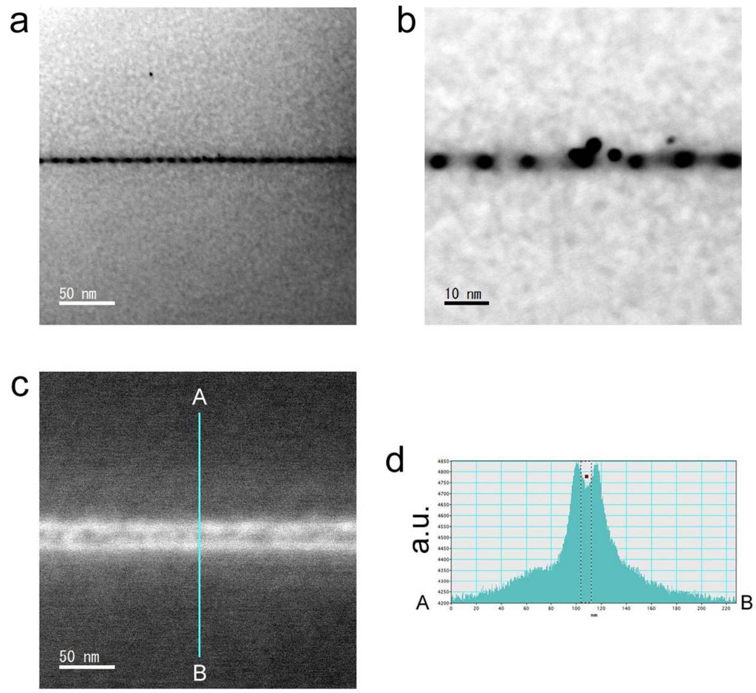

Figure S5. Plan-view STEM characterizations of the linear surface pits. (a) A STEM ADF image of a dense sequence of surface pits fabricated in a thinner area of the thin plate specimen with the same experimental conditions as used to fabricate the 440 nm corral. (b) Partial enlargement shows the defects are composed of a dotted sequence of surface pits of a few nanometer in diameter. (c) A STEM ADF image of an edge of the 800 nm triangular corral as shown in Figure 4. (d) A line profile across the line between A and B as indicated in (c).

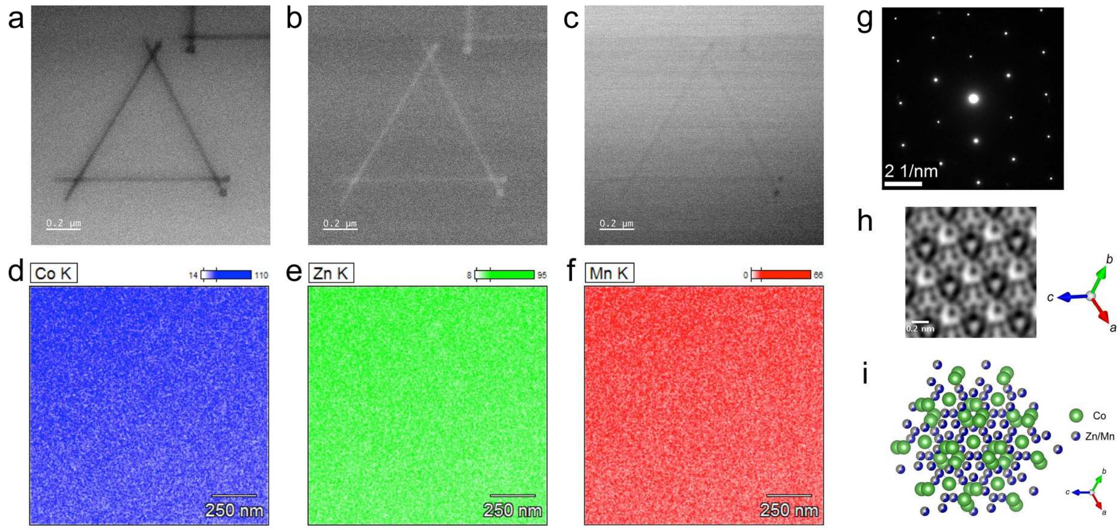

Figure S6. Plan-view STEM/EDX characterizations of the triangular corrals fabricated in a thin plate prepared from a bulk polycrystal of $Co_8Zn_8Mn_4$. (a) Annular bright field (ABF), (b) low angle annular dark field (LAADF), (c) high angle annular dark field (HAADF) STEM images of the triangular corral. (d)-(f) STEM energy dispersive X-ray (EDX) analysis of the triangular corral showing no apparent local precipitations of specific atomic species (Co, Zn, Mn) over the fabricated area. (g) A TEM diffraction pattern, (h) a principal component analysis (PCA)-averaged (Matsumoto, T. *et al. Nano Lett.* **2013**, *13*, 4594) ABF STEM image obtained from a thinner part of the thin plate, and (i) atomic model viewed from [111] zone-axis drawn by using VESTA software (Momma, K. and Izumi, F. J. Appl. Crystallogr. **2011**, *44*, 7638).

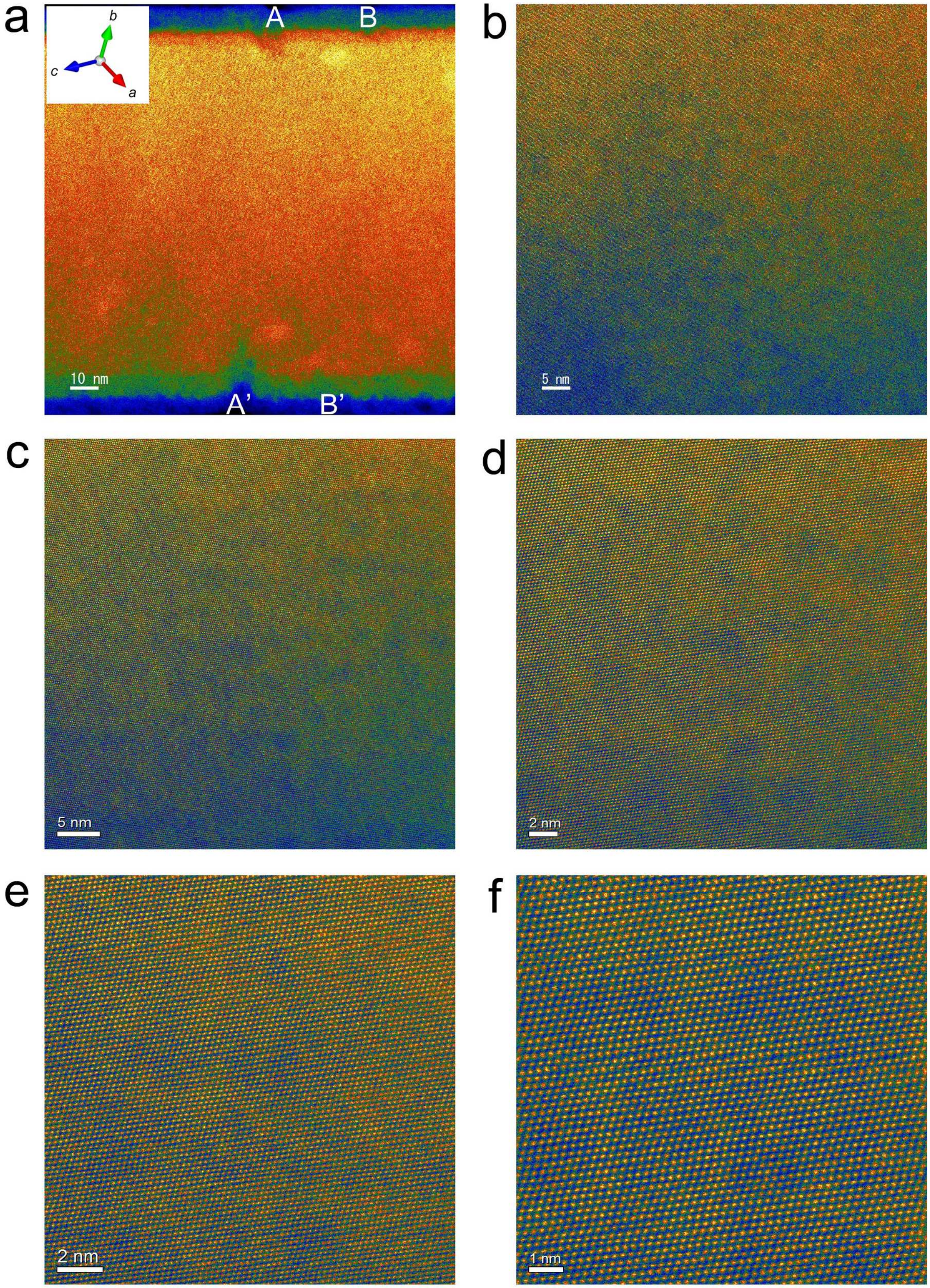

Figure S7. Cross-sectional STEM characterizations of the linear surface pits. (a) A pseudo-color low-magnification image showing the surface pits (designated as A and B) on the top (beam entrance) surface and those (designated as A' and B') on the bottom (beam exit) surface of the dummy thin plate specimen. (b)-(f) A sequence of zoom-in images around the area along A-A'. No apparent damage can be noticed along A-A' while surface pits are observed on the both surfaces as shown in Figure 6 in the main text.

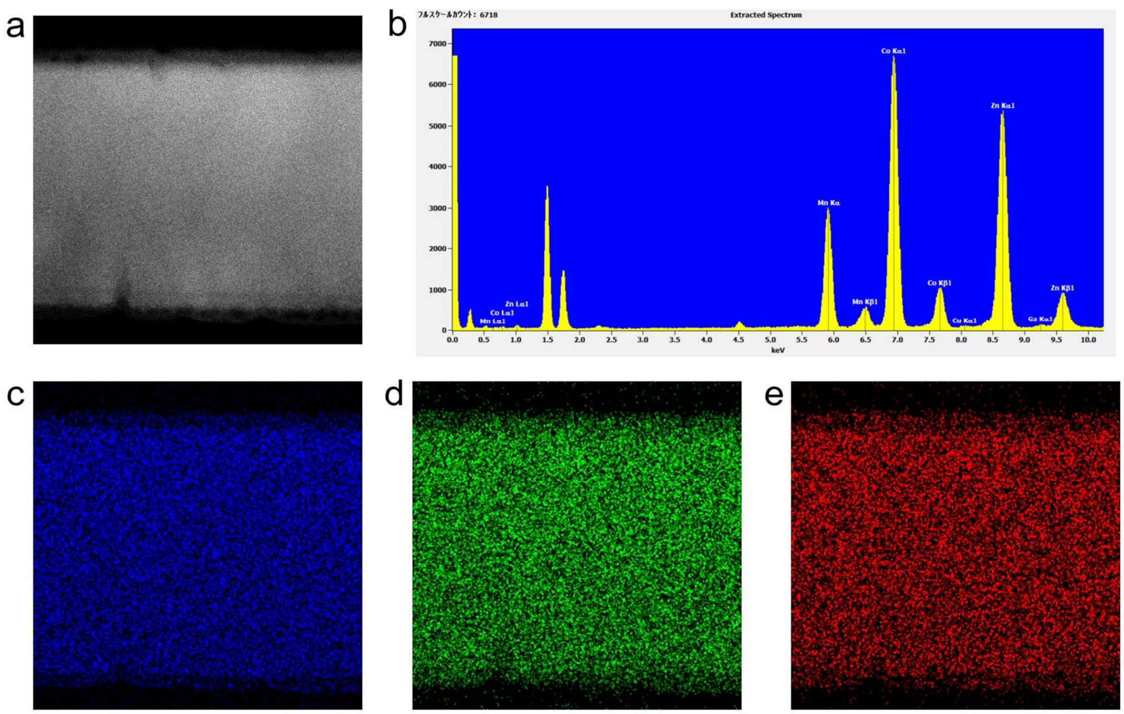

Figure S8. Cross-sectional STEM/EDX characterizations of the linear surface pits. (a) STEM HAADF image, (b) spectrum, (c) Co, (d) Zn, and (e) Mn compositional maps.

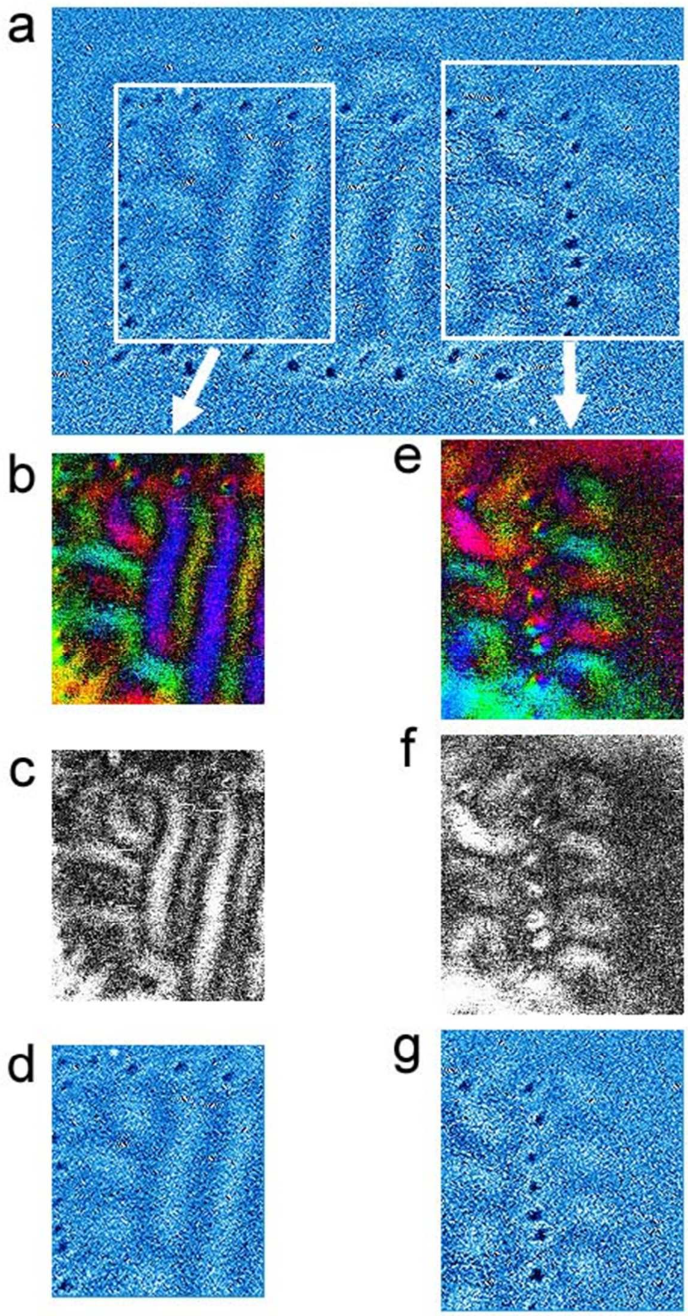

Figure S9. Partially reconstructed DPC STEM images as shown in Figure 2c demonstrating that what is observed is not helical stripes but strongly deformed skyrmions. (a) The helicity image as shown in Figure 2c. (b) Partially reconstructed in-plane magnetic field vector map, (c) in-plane magnetic field intensity, (d) pseudo-color magnetic helicity image from the left rectangular region indicated in (a). (e) Partially reconstructed in-plane magnetic field vector map, (f) in-plane magnetic field intensity, (g) pseudo-color magnetic helicity image from the right rectangular region indicated in (a).

Movie S1. A movie showing the sequential observations of the magnetic skyrmion state inside the rectangular corral created by a focused electron beam as shown in Figure 2 and Figure S3.

Movie S2. A movie showing the sequential observations of the magnetic skyrmion state inside the 800 nm triangular corral created by a focused electron beam as shown in Figure 4 and Figure S4.

Movie S3. Movie S2 repeated several times back and forth at a faster speed focused on the triangular part only.